Raman Studies of Alkali-Metal Doped A_xC_{60} Films (A = Na, K, Rb, and Cs; x = 0, 3, and 6)

S. J. DUCLOS,* R. C. HADDON, S. GLARUM, A. F. HEBARD, K. B. LYONS

The room temperature Raman spectra of the intramolecular modes between 100 cm^{-1} and 2000 cm^{-1} are reported for alkali-metal doped A_xC_{60} films. For A = K, Rb, and Cs, phase separation is observed with the spectra of C_{60}, K_3C_{60}, K_6C_{60}, Rb_3C_{60}, Rb_6C_{60}, and Cs_6C_{60} phases reported. The x = 3 phases show only three Raman active modes: two of A_g symmetry and only the lowest frequency H_g mode. The other H_g modes regain intensity in the x = 6 films, with several mode splittings observed. For A = Na, such phase separation is not clearly observed, and reduced mode shifts are interpreted as due to incomplete charge transfer in these films.

CONDUCTING (*1*) AND SUPERCONducting (*2*) compounds of A_xC_{60} ($0 \leq x \leq 6$) have recently been prepared by intercalating alkali metals (A) into both powders and films of C_{60} buckminsterfullerene (*3–4*). Raman spectroscopy is an optical probe of the normal mode frequencies of the C_{60} cage, which are influenced by C–C bond strengths, as well as the electron-phonon coupling important to superconductivity. This report presents Raman spectra of the C_{60} intramolecular modes for all dopant phases observed in films. The spectra show a significant dependence on dopant phase, and represent a convenient optical probe of phase separation in films. Shifts in frequency of these modes as x is increased from 0 to 6 can be attributed to changes in the C–C bonds as the anti-bonding states of the C_{60} molecule become occupied. The relatively high superconducting transition temperatures (18 K to 33 K) (*2, 5–8*) have stimulated interest in the strength of the electron-phonon coupling in the A_3C_{60} superconductors. The intramolecular phonon modes observed in these Raman spectra are of particular interest owing to their calculated strong scattering of electrons at the Fermi-surface (*9–10*). Thus the Raman spectra presented here lead to insights on the binary phase diagram of doped C_{60} films, changes in the intramolecular bonding with doping, and the superconducting mechanism of the A_3C_{60} compounds.

The unpolarized Raman spectra were excited by 50 W cm^{-2} (15 mW incident power) of the 514.5 nm Ar ion laser line on approximately 100 μm by 300 μm spots (Fig. 1). A monochromator was used to eliminate laser plasma lines from the spectra. Light was collected in a 45° back scattering geometry, and dispersed by a 3/4-m Spex double spectrometer with 7 cm^{-1} spectral resolution. Light was detected with a Hamamatsu R585 photomultiplier tube (PMT) and photon counting electronics. Scanning speeds of 10 cm^{-1} per minute were used, and the spectra presented are an average of three scans.

The C_{60} used in the present experiments was first purified by chromatography and reprecipitated in hexane to remove organic contaminants. Films were then grown by sublimation at 425°C for 6 minutes onto the inner surface of evacuated Suprasil tubes of 2-mm inside diameter. X-ray diffraction peak widths indicate a crystallite size of approximately 50 to 60 Å in these films. The Raman spectrum of the Suprasil tube has been measured under the same conditions, and none of the features reported here, unless otherwise stated, can be attributed to it. Doping was accomplished by inserting alkali metal into the tube in a He glove box, sealing in a vacuum of $<10^{-3}$ torr, and heating the entire tube isothermally (*11*). The superconducting transition temperature, as measured by microwave absorption, of the K- and Rb-doped films was increased by annealing the film portion of the tube after doping. The total doping times and temperatures, and annealing times and temperatures are summarized in Table 1. This resulted in either two (Cs) or three (Na, K, and Rb) visibly sharp bands along the axis of the tube (Fig. 1B). Stability of the doped materials was confirmed by scanning the high frequency A_g mode before and after 24 hours of laser irradiation under the same focus conditions. The Na-doped film showed several anomalous features, and will be discussed separately at the end of this report.

The stoichiometry of the resulting bands has been determined in the following manner. A film that we homogeneously doped with K using the geometry of Haddon *et al.* (*1*) was simultaneously probed with both Raman spectroscopy and van der Pauw four-probe resistivity measurements. The spectrum of the material at the resistivity minimum, identified as K_3C_{60} by previous Rutherford backscattering spectroscopy (RBS) measurements (*12*), matched that found for the middle band of the K- and Rb-doped films grown in Suprasil tubes. Upon further doping, the spectrum acquired at the resistivity maximum, identified as K_6C_{60} by RBS measurements (*12*), matched that found in the upper band of the K-, Rb-, and Cs-doped films. The position of the superconducting phase, which we infer to be A_3C_{60}, was also measured by low-temperature microwave absorption (*11*). For the K- and Rb-doped films this was found to be the same band as that identified as A_3C_{60} by the simultaneous Raman and resistivity measurements. The banding and distinct phases observed here are consistent with the phase separation observed in bulk samples by x-ray diffraction and NMR (*13*). We note that no evidence of the A_4C_{60} (*14*) or Cs_3C_{60} (*7*) phases has been observed in these films.

A spectrum of pristine C_{60} sublimed in a tube and unexposed to air, O_2, or alkali metal was taken (Fig. 2). We have previously shown (*15*) that exposure of vacuum-grown films to either air or oxygen alters the spectrum, especially in the frequency region of the symmetric A_g mode at 1458 cm^{-1}. In previous experiments (*15*) the Si substrate inhibited the identification of modes near 520 cm^{-1} and 950 cm^{-1} to 1000 cm^{-1}. In the present experiments, the Si substrate has been eliminated and we can identify the mode at 522 cm^{-1} and the broad feature between 950 cm^{-1} and 1000 cm^{-1} as due to C_{60}. The broad feature may result from a two phonon process involving the 490

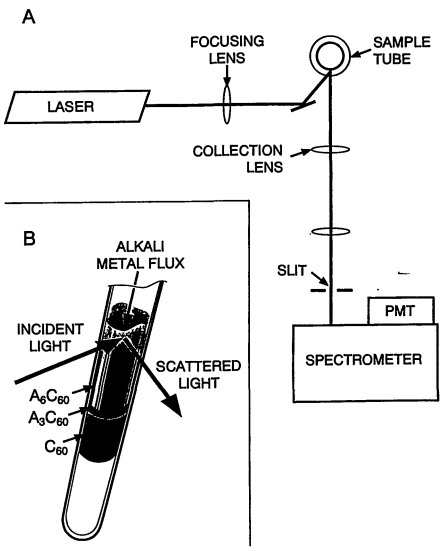

Fig. 1. (**A**) Schematic of the Raman spectrometer used in the present experiments. (**B**) Drawing of the sample tube after alkali metal doping, showing bands of different alkali stoichiometry in the film on the inside surface of the tube.

AT&T Bell Laboratories, Murray Hill, New Jersey 07974.

*To whom correspondence should be addressed.

Table 1. Total doping and annealing times and temperatures for the A_xC_{60} films used in this study. No annealing of the Cs-doped film was done, as it showed no evidence of a Cs_3C_{60} phase.

Alkali metal	Doping		Annealing	
	Temperature (°C)	Time (hours)	Temperature (°C)	Time (hours)
Na	190	4	180	1.5
K	130	1.7	220	32
Rb	100	7.7	120	6
Cs	70	16.4	—	—

cm^{-1} mode. In addition, modes are observed in the 275 cm^{-1} region, which closely corresponds to the calculated frequency of the lowest frequency H_g mode. Splittings in this frequency region, as well as in the 700 cm^{-1} to 775 cm^{-1} range, may be attributable to loss of symmetry of the C_{60} molecule owing to interactions with its neighbors in the solid state. Depolarization ratios of the modes of the pristine material are consistent with the mode interpretations of Bethune *et al.* (*16*), who assign the 1458 cm^{-1} peak to the pentagonal-pinch A_g mode, and the 488 cm^{-1} peak to the A_g symmetric breathing mode, and the others as H_g modes, including the low-frequency C_{60} squashing mode. The full width at half maximum (FWHM) of the 1458 cm^{-1} mode is 15 cm^{-1}, and Tolbert *et al.* (*17*) attribute the anomalous width to rotational-vibrational coupling. The line in our data may be further broadened by the loss of momentum conservation caused by grain boundaries in our microcrystalline films. Incorporation of O_2 into these microcrystalline films results in an intense peak at 1469 cm^{-1} with a resolution-limited FWHM. The Raman spectra of the alkali-doped phases did not depend on whether or not the starting film had been exposed to air.

We now consider films doped to the A_3C_{60} phase. Raman spectra were obtained for K_3C_{60} (T_c = 18 K) and Rb_3C_{60} (T_c = 24 K) (Fig. 3). The striking feature of these spectra is their simplicity. Only three modes are observed, the two A_g modes and the lowest frequency H_g mode. Further, there is no dependence of the spectra on alkali dopant, indicating no A-C_{60} mode is observed above 100 cm^{-1}. Spectra taken on a variety of K- and Rb-doped samples indicate that the A_g mode frequency in A_3C_{60} is 1445 ± 2 cm^{-1}. The FWHM of this mode is 9 cm^{-1}, which is 6 cm^{-1} less than the value for the pristine material. This reduction is likely due to the stationary orientation of the C_{60} molecules on the time scale of the Raman scattering process, and is similar to the reduction observed in pristine C_{60} as the molecules freeze at low temperatures (*17*). This result is consistent with recent NMR and x-ray diffraction results that indicate the molecules are jumping between symmetry-equivalent orientations in the K_3C_{60} material at room temperature (*13*). Finally, we point out that the lowest frequency H_g mode appears to remain, although it is significantly broadened.

We have considered several possible explanations for the disappearance of most of the H_g modes. First, the addition of alkali metal atoms to the lattice will introduce symmetry reduction due to A-C_{60} interactions, which will tend to broaden the H_g modes as their degeneracy is broken. However, on the scale of our resolution these effects should be small and, as discussed below, further doping results in a reappearance of many of these lines, which argues against the intensity reduction solely rising from symmetry breaking. A second explanation involves resonant enhancement of the A_g lines as the electronic structure of the solid is altered during doping, as well as a reduction in overall intensity due to decreased penetration depth of the laser into the metallic material. A factor of 5 decrease in penetration depth would render all of the H_g modes below 1400 cm^{-1} unobservable. Third, recent treatments (*9–10*) of the electron-phonon coupling in doped C_{60} indicate that the H_g modes couple more strongly than do the A_g modes. As discussed by Allen (*18*), such coupling leads to a broadening of the affected modes, and for A_3C_{60} will result in a greater broadening for the H_g modes. An assessment of the relative merits of these explanations will be possible only after optical work is performed on the A_3C_{60} materials to determine the penetration depth and the possible effects of resonant enhancement on the observed modes.

Figure 4 shows the Raman spectra of K_6C_{60}, Rb_6C_{60}, and Cs_6C_{60}. The high frequency A_g mode is now at 1430 ± 1 cm^{-1}, and has a resolution-limited FWHM of 7 cm^{-1}. The further narrowing of this mode may be due to continued freezing out of the rotational-vibrational coupling, as NMR (*13*) and synchrotron x-ray (*19*) results indicate that the molecules are completely frozen at room temperature in K_6C_{60}. The shift of the A_g mode with doping in the solid appears to be linear at 5 cm^{-1} per electron reduction of C_{60}, and is a convenient probe of reduction state of the molecule in the solid (*1*).

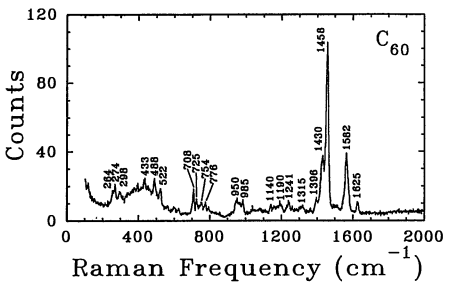

Fig. 2. Room temperature unpolarized Raman spectrum of a pure C_{60} film grown on the inside surface of a Suprasil tube without exposure to air. A broad background between 200 cm^{-1} and 500 cm^{-1} is from the Suprasil tube. The peak at 488 cm^{-1} lies very near a similar weaker feature in SiO_2, but has been observed in samples deposited on Si (*15*). The laser power density (50 W/cm^2 at 514.5 nm) is the same as for the spectra in Figs. 3 and 4.

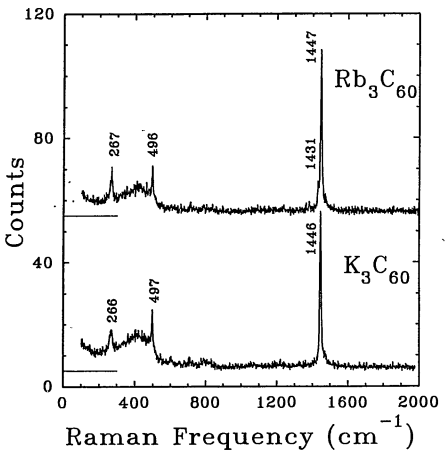

Fig. 3. Room temperature unpolarized Raman spectra of A_3C_{60} (A = Rb and K). Both spectra are on the same scale, but are shifted vertically for clarity. The broad background between 200 cm^{-1} and 500 cm^{-1} is from the Suprasil tube. The shoulder on the low frequency side of the 1447 cm^{-1} peak in Rb_3C_{60} is likely due to a small contamination of Rb_6C_{60}.

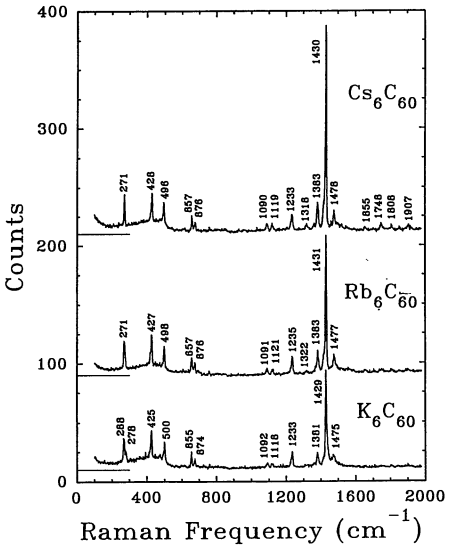

Fig. 4. Room temperature unpolarized Raman spectra of A_6C_{60} (A = Cs, Rb, and K). All of the spectra are on the same scale, but are shifted vertically for clarity. The broad background between 200 cm^{-1} and 500 cm^{-1} is from the Suprasil tube.

The similarity between the A_6C_{60} spectra doped with different alkali metals again indicates that the observed modes are due only to the C_{60} molecule, and that there are no observable A-C_{60} modes above 100 cm^{-1}. The mode at 270 cm^{-1} has a resolution-limited FWHM for Cs_6C_{60}, is broadened in Rb_6C_{60}, and is a doublet in K_6C_{60}. The high-frequency mode of the doublet may result from a two-phonon process involving a low energy–A-C_{60} mode, the frequency of which will increase as the ion mass is reduced. Finally, we also point out that the four modes observed above 1600 cm^{-1} in Cs_6C_{60} (and weakly in Rb_6C_{60} and K_6C_{60}) appear to be sum modes of the two lowest frequency H_g modes (271 cm^{-1} and 428 cm^{-1}) and the two highest frequency H_g modes (1383 cm^{-1} and 1478 cm^{-1}). If this is the case, it is not clear that these modes should be broadened in the same way as the zone center (one-phonon) modes by the electron phonon coupling (*9–10*).

The Raman spectra of Na_xC_{60} are consistent with the above results with the following exceptions. Although banding was observed in these films upon doping, intermediate values of the A_g mode frequency were observed between 1448 cm^{-1} and 1455 cm^{-1}. Also, a time dependence of this mode frequency has been observed in the laser beam at the power densities used in the studies of the K-, Rb-, and Cs-doped films. These results indicate that Na-doped C_{60} either does not phase separate in Na_xC_{60} with $0 \leq x \leq 3$ or that phases other than $x = 0$ and $x = 3$ are stable. For Na_6C_{60} the A_g mode is at 1434 cm^{-1}, significantly higher than the 1430 ± 1 cm^{-1} observed in the other A_6C_{60} materials. This is consistent with incomplete electron transfer in Na_xC_{60}, which may be responsible for the lack of superconductivity above 4 K (*11*). Further work is needed to clarify the phase diagram and electronic structure of the Na_xC_{60} compounds.

REFERENCES AND NOTES

1. R. C. Haddon *et al.*, *Nature* **350**, 320 (1991).
2. A. F. Hebard *et al.*, *ibid.*, p. 600.
3. H. W. Kroto, J. R. Heath, S. C. O'Brien, R. F. Curl, R. E. Smalley, *ibid.* **318**, 162 (1991).
4. W. Krätschmer, L. D. Lamb, K. Fostiropoulos, D. R. Huffman, *ibid.* **347**, 354 (1990).
5. M. J. Rosseinsky *et al.*, *Phys. Rev. Lett.* **66**, 2830 (1991).
6. K. Holczer *et al.*, *Science* **252**, 1154 (1991).
7. S. P. Kelty, C.-C. Chen, C. M. Lieber, *Nature* **352**, 223 (1991).
8. K. Tanigaki *et al.*, *ibid.*, p. 222.
9. C. M. Varma, J. Zaanen, K. Raghavachari, *Science* **254**, 989 (1991).
10. M. A. Schluter, M. Lannoo, M. K. Needels, G. A. Baraff, in preparation.
11. S. H. Glarum, S. J. Duclos, R. C. Haddon, in preparation.
12. G. P. Kochanski, A. F. Hebard, R. C. Haddon, A. T. Fiory, in preparation.
13. R. Tycko *et al.*, *Science* **253**, 884 (1991).
14. R. M. Fleming *et al.*, *Nature* **352**, 701 (1991).
15. S. J. Duclos, R. C. Haddon, S. H. Glarum, A. F. Hebard, K. B. Lyons, *Solid State Commun.*, in press.
16. D. S. Bethune *et al.*, *Chem. Phys. Lett.* **179**, 181 (1991).
17. S. H. Tolbert, A. P. Alivistatos, H. Lorenano, M. Kruger, R. Jeanloz, in preparation.
18. P. B. Allen, *Phys. Rev. B* **6**, 2577 (1972).
19. O. Zhou *et al.*, *Nature* **351**, 462 (1991).

20. We thank R. M. Fleming, M. Schluter, P. Sulewski, R. Tycko, and C. Varma for valuable discussions.

2 October 1991; accepted 29 October 1991

Molecular Architecture and Electrostatic Properties of a Bacterial Porin

M. S. WEISS, U. ABELE, J. WECKESSER, W. WELTE, E. SCHILTZ, G. E. SCHULZ*

The integral membrane protein porin from *Rhodobacter capsulatus* consists of three tightly associated 16-stranded β barrels that give rise to three distinct diffusion channels for small solutes through the outer membrane. The x-ray structure of this porin has revealed details of its shape, the residue distributions within the pore and at the membrane-facing surface, and the location of calcium sites. The electrostatic potential has been calculated and related to function. Moreover, potential calculations were found to predict the Ca^{2+} sites.

GRAM-NEGATIVE BACTERIA PROTECT themselves from hostile environments by an outer membrane. This membrane, however, has to be permeable to polar, low molecular mass solutes including nutrients. For this purpose it contains channel-forming proteins called porins, which are usually trimeric with relative subunit masses between 30,000 and 50,000 and solute exclusion limits around 600 daltons (*1, 2*). Spectroscopic (*3*) and electron microscopic studies (*4, 5*) have yielded a rather general description of their architecture. Several porins have been crystallized and subjected to x-ray diffraction analyses (*6–10*). Among these, the crystals of porin from the photosynthetic bacterium *Rhodobacter capsulatus* strain 37b4 could be analyzed to atomic resolution (*8, 11–14*). We describe this porin with respect to its shape, its pore properties, its outer surface, and its electrostatic properties.

The present crystallographic *R* factor of the porin model (*15*) is 0.191 in the resolution range from 10 to 1.8 Å. As displayed in Fig. 1, a porin subunit consists of 16 β strands with lengths ranging from 6 to 17 residues. The 16 strands form a completely antiparallel β barrel, in which all strands are connected to their neighbors. Three of the 15 connecting loops contain short α helices. The seven loops at the bottom of the barrel (Fig. 1) are short (two to five residues) whereas the eight loops at the top end are generally longer (5 to 44 residues, with an average of 14 residues). The tilting angles of the β strands against the trimer axis, which coincides with the membrane normal, vary from 30° to 60°. The model contains three calcium ions: two are located within the pore (Ca-I and Ca-II) and the third one (Ca-III) at the subunit interface. The presumed detergent molecule of the model binds in a hydrophobic pocket below helix α3.

The shape of a porin subunit is represented with a low-resolution electron density map displayed at the 1σ level. A cut through the center of one subunit yields two halves depicted side by side in Fig. 2. Four cutting areas are created: no. 1, the β barrel with a short height at the subunit interfaces near the molecular threefold axis; no. 2, the β barrel at its maximum height at the membrane-facing side; no. 3, the 44-residue loop between strands β5 and β6 inside the β barrel; and no. 4, the second largest loop (20 residues between strands β11 and β12) forming a small globule at the top end of the β barrel.

The association of porin subunits to the trimer can be done by a superposition of both indicated axes, followed by a rotation of the left-hand side by 60° around this axis. This connects the rear β barrel walls at the heights of the indicated discontinuous lines (see Fig. 5 for verification). Thus, a common channel of the three subunits is formed that extends from the upper discontinuous line to the upper end of section area no. 1. This common channel leads into three distinct eyelets (one per subunit) that define

M. S. Weiss, U. Abele, E. Schiltz, G. E. Schulz, Institut für Organische Chemie und Biochemie, Albertstrasse 21, D-7800 Freiburg im Breisgau, Federal Republic of Germany.
J. Weckesser, Institut für Biologie II, Mikrobiologie Schänzlestrasse 1, D-7800 Freiburg im Breisgau, Federal Republic of Germany.
W. Welte, Institut für Biophysik und Strahlenbiologie, Albertstrasse 23, D-7800 Freiburg im Breisgau, Federal Republic of Germany.

*To whom correspondence should be addressed.